Biochemical and Biophysical Research Communications 435 (2013) 526–532

Contents lists available at SciVerse ScienceDirect

Biochemical and Biophysical Research Communications

journal homepage: www.elsevier.com/locate/ybbrc

# Aberrant methylation and loss of *CADM2 tumor suppressor* expression is associated with human renal cell carcinoma tumor progression

Wei He [a,b], Xuesong Li [a,b], Shuping Xu [c], Junkui Ai [d], Yanqing Gong [a,b], Jennifer L. Gregg [d], Ruili Guan [a,b], Wei Qiu [a,b], Dianqi Xin [a,b], Jeffrey R. Gingrich [d], Yinglu Guo [a,b,*], Guimin Chang [d,*]

[a] Department of Urology, Peking University First Hospital and the Institute of Urology, Peking University, No. 8, Xishiku Street, Xicheng District, Beijing 100034, China
[b] National Urological Cancer Center, Beijing 100034, China
[c] Department of Pharmacology and Chemical Biology, University of Pittsburgh School of Medicine, E1354 BST, Pittsburgh, PA 15261, USA
[d] Department of Urology, University of Pittsburgh, 5200 Centre Ave., Pittsburgh, PA 15232, USA

ARTICLE INFO

*Article history:*
Received 16 April 2013
Available online 3 May 2013

*Keywords:*
*CADM2*
Renal cell carcinoma
Methylation
Tumor suppressor

ABSTRACT

Cell adhesion molecules (CADMs) comprise a protein family whose functions include maintenance of cell polarity and tumor suppression. In this report, we show that the *CADM2* gene is repressed in human clear renal cell carcinoma by DNA promoter hypermethylation and/or loss of heterozygosity. Moreover, the loss of *CADM2* expression is associated with a higher tumor pathology stage ($p < 0.05$). The re-expression of *CADM2* in the renal cancer cell line 786-O significantly suppressed tumor cell growth *in vitro* and in mouse xenografts by a G1 phase cell cycle arrest and the induction of apoptosis. Lentivirus-mediated *CADM2* expression also significantly suppressed cancer cell anchorage-independent growth and invasion. Furthermore, the inhibition of endogenous *CADM2* expression using siRNAs induced a tumorigenic phenotype in polarized non-tumorigenic MDCK cells. Thus, we conclude that *CADM2* functions as a novel tumor suppressor and may serve as a potential therapeutic target for human renal cell carcinoma.


## 1. Introduction

Renal cancer accounts for approximately 2% of all cancers worldwide, and more than 200,000 new cases of renal cancers are diagnosed annually [1]. Approximately, 75% of renal cancers are classified as clear renal cell carcinoma (cRCC) [2]. Although surgery and targeted therapies improve the treatment of cRCC, the prognosis of cRCC remains poor [1]. Accurate prognostic tests as well as more effective treatment strategies require a better understanding of the molecular events that underlie cRCC progression [3].

Recent studies suggest that the expression of cell adhesion molecules (CADMs), a protein family that may have a role in cancer progression, is lost as a result of promoter hypermethylation [4,5]. Moreover, hypo-expression of *CADM2* gene expression has been observed in prostate cancer [6], ovarian cancer [7], lymphoma and melanoma [8,9]. Thus, this study sought to characterize *CADM2* expression in cRCC. Here, we showed that *CADM2* expression was reduced in cRCC, and re-expression suppressed cancer cell tumorigenicity *in vitro* and *in vivo*, implicating that *CADM2* is a novel tumor suppressor candidate in cRCC.

## 2. Materials and methods

### 2.1. Cell lines and tissue samples

The human renal cancer cell lines, 786-O, OS-RC-2 and CAKI-1, were purchased from the National Platform of Experimental Cell Resources for Sci-Tech (Beijing, China), and maintained in RPMI1640 or McCoy's 5A containing 10% GIBCO FBS (Carlsbad, CA) with 1% antibiotics. HEK-293 cells were grown in DMEM/HG supplemented with FBS and antibiotics. The human kidney proximal tubular epithelial cells, HK-2, was purchased from ATCC (Manassas, VA) and cultured in KSF medium with bovine pituitary extract and epidermal growth factor (Invitrogen, Carlsbad, CA). All cells were maintained at 37 °C in a humidified incubator with 5% $CO_2$.

Primary tumor tissues (T), paired adjacent normal kidney tissues (N) specimens and clinical data were obtained from 61 histo-

*Abbreviations:* CADMs, cell adhesion molecules; cRCC, clear renal cell carcinoma; RT-qPCR, reverse transcription quantitative polymerase chain reaction; MSP, methylation-specific polymerase chain reaction; BSP, bisulfite sequencing polymerase chain reaction.

* Corresponding authors. Address: Department of Urology, Peking University First Hospital and the Institute of Urology, Peking University, No. 8, Xishiku Street, Xicheng District, Beijing 100034, China. Fax: +86 10 66551028 (Y. Guo), fax: +1 412 623 3907 (G. Chang).

*E-mail addresses:* guoyingluu@gmail.com (Y. Guo), guc6@pitt.edu, guiminchang@yahoo.com (G. Chang).

0006-291X/$ - see front matter © 2013 Elsevier Inc. All rights reserved.
http://dx.doi.org/10.1016/j.bbrc.2013.04.074

logically classified cRCC patients that received radical nephrectomies or partial renal resection in the Urology Department of the Peking University First Hospital. Informed consent was obtained from all patients, and this study was approved by the institutional review board of the Peking University First Hospital. The pathological stage was assessed by two experienced urological pathologists, according to the AJCC 2009 classification system.

### 2.2. Peptides synthesis and antibody generation

Peptides synthesis and antibody used for Immunohistochemistry and Western blot analysis were carried out as previously described [6]. The following synthetic peptide corresponding to amino acids 426–444 of CADM2 were produced: COOH-terminal CIINAEGSQVNAEEKKEYFI. After conjugation to keyhole limpet hemocyanin (KLH), the resulting antibodies were affinity purified using the immunizing peptide (Research Genetics, Huntsville, AL).

### 2.3. Immunohistochemistry and Western blot analysis

The immunohistochemistry was carried out as previously described [6]. Tissue sections were stained using a DAKO Immunohistochemistry Kit (DAKO, Carpinteria, CA) and visualized using an Olympus microscope. Protein lysates were prepared by homogenization in RIPA lysis buffer containing PSFM and 30 μg was separated by SDS–PAGE. The immunoreactive bands were visualized by Immobilon™ Western Kit (Millipore, Billerica, MA) using SYNGENE G:BOX imaging system (Frederick). Semi-quantification of the bands was performed using ImageJ software.

### 2.4. Quantitative real-time PCR (qPCR)

Total RNA from cultured cells and frozen specimens was isolated using TRIZOL reagent (Invitrogen), and 2 μg total RNA was reverse-transcribed using the Reverse Transcription System (Promega, Madison, WI). qPCR was performed using the Applied Biosystem 7500-fast with SYBR Green PCR Mix (Roche, Indianapolis, IN). Each reaction was performed in triplicate with each primer sets (Supplementary Table 1). *CADM2* expression was normalized to human *β-Actin* expression using the ΔΔCT method.

### 2.5. Methylation-specific PCR (MSP) and bisulfite sequencing PCR (BSP)

Genomic DNA was extracted using a DNA extraction kit (Qiagen, Gaithersburg, MD); 1 μg was used for bisulfite treatment as previously described [6]. Ten ng modified genomic DNA was amplified with MSP primer sets (Supplementary Table 1) using a Hotstart PCR Mix (Promega) and the following reaction conditions: 94 °C for 6 min; 40 cycles of 94 °C for 30 s, 54 °C for 30 s, and 72 °C for 30 s; and 72 °C for 5 min. PCR products were analyzed in 1.5% agarose gels stained with ethidium bromide. The BSP reaction was performed as previously described [6] using primers in Supplementary Table 1. The PCR products were purified and cloned into PCR2.1-TA cloning vector (Invitrogen), and a minimum of six positive clones from each product were selected for sequencing.

### 2.6. Demethylation analysis

786-O cells were seeded in six-well plates at a concentration of $1 \times 10^5$ cells per well, grown for 24 h, and then treated with 0, 2, 5, or 10 μM 5-Aza-2′-deoxycytidine (5-Aza-dC, Sigma, St. Louis, MO) for 4 days. Cells were cultured with or without 300 nM Trichostatin A (Sigma) for the final 24 h. RNA was isolated for RT-PCR analysis, and DNA was extracted for *CADM2* MSP.

### 2.7. Loss of heterozygosity (LOH) analysis

Genomic DNA (50 ng) from the paired tumor and adjacent normal tissues were amplified by PCR for LOH analysis as previously described [10], using fluorescent-labeled primers (Supplementary Table 2). Five human polymorphic short tandem sequence markers within a 17 Mb region at 3p12.1–3 around the *CADM2* were chosen. Molecular size and peak height were analyzed with Genetic Profiler v.1.0 software. LOH was determined using the calculation method described by Powell et al. [11], which defined LOH using a normalized allele ratio $\leqslant 0.6$.

### 2.8. Construction of CADM2-expressing lentivirus

Previous report showed that the *CADM2* gene encodes several mRNA isoforms [6], including *CADM2* missing exon 8 isoform (*CADM2-M8*) and the full-length isoform (*CADM2-FL*). *CADM2-M8*- and *CADM2-FL*-expressing lentiviruses were generated using the GV177 system (Genecheme, Shanghai, China). The recombinant virus was purified, characterized, and titrated by qPCR, and its infectivity was detected after transduction at increasing multiplicity of infection (MOI).

### 2.9. In vitro cell proliferation, invasion, apoptosis, cell cycle and soft agar colony formation assays

After infection, 786-O cell proliferation was determined using a cell counting kit-8 (Keygen) following manufacturer's instructions. This assay was performed in triplicate. For the invasion assay, infected 786-O cells were seeded on transwells with 8-μm pores (Millipore, Billerica, MA), coated with Matrigel (BD, San Antonio, TX). After 48 h, adherent cells on the top surface of the filter were removed. Cells were fixed with 4% paraformaldehyde and stained with crystal violet, and the number of cells on the lower surface was counted.

To detect apoptosis, 786-O cells ($1 \times 10^5$ cells per well) were seeded in six-well plates and infected with lentivirus at MOI 40. After 3 days, cells were stained with Annexin V-FITC (Keygen) and analyzed using BD Influx™ cell sorter (BD). Cell cycle was analyzed using the cell cycle detection kit (Keygen). For colony formation analysis, $1 \times 10^4$ infected 786-O cells were mixed with 0.7% top agar (Sigma) in 60 mm plates coated with 1.2% base agar. After 2 weeks, the cells were stained with crystal violet. The assay was performed in triplicate.

### 2.10. In vivo tumorigenesis assay

BALB/$c^{nu/nu}$ mice, which were 4–6 weeks-old and 18–25 g (Vitalriver, Beijing, China), were maintained in a specific pathogen-free environment and randomly divided into the following four treatment groups: control (786-O cells), empty mock (786-O cells infected with an empty vector control), M8, and FL (CADM2-expressing 786-O cells, at MOI 40 respectively) groups, four mice for each group. Mice received subcutaneous cell injections ($5 \times 10^6$ cells in 100 μL PBS) in the armpit. Tumor diameter was measured every third day after day 10, and tumor volume was calculated using the following formula: length $\times$ $(\text{width})^2/2$. Mice were sacrificed after 30 days. Animals were maintained and experiments were carried out according to the institutional guidelines established for the Animal Facility Center at Peking University.

### 2.11. CADM2 siRNA knockdown

The CADM2 target sequence (5′-AGCGGCTGCTTCAAAGAATAA-3′) and predesigned siRNA inserts were obtained using the

GenScript siRNA Target Finder and siRNA Construct Builder programs with the Ensembl canine sequence (ENSCAFG00000007806). A siRNA specific for luciferase (5′-CGTACGCGGAATACTTCGA-3′) was used as a negative control. The siRNA primers were annealed with the pRNAT vector, which has the *green fluorescence protein (GFP)* gene. After transfection of pRNAT-CADM2 or pRNAT-luciferase siRNAs, MDCK cells, a polarized canine kidney epithelial cell line, were selected using G418, and stable clones were pooled for further experiments. To determine the degree of CADM2 silencing, RT-PCR and Western blot analyses were performed. Colony formation was determined as described above. For Matrigel invasion assays, control or CADM2 siRNA-transfected MDCK cells ($1 \times 10^5$ cells/well) were seeded onto 24-well plates coated with Matrigel. After 18 h, the cells were imaged using an inverted phase contrast microscope. All results are representative of at least three independent experiments.

### 2.12. Statistical analysis

Statistical analysis was performed using SPSS 20.0 (SPSS, Chicago, IL). A paired *t*-tests were applied to compare the significance between the tumor and adjacent normal tissue pairs. The relationship between *CADM2* methylation and clinical information and pathology was evaluated by a Kruskal–Wallis one-way ANOVA to compare the mean values within pT staging of renal cancer. A *P*-value < 0.05 was considered statistically significant.

## 3. Results

### 3.1. CADM2 expression is reduced in both renal cancer cell lines and human cRCC

Western blot analyses revealed that CADM2 protein band was predominantly expressed in HK-2 and HEK-293 and decreased in primary tumor tissues as compared with the corresponding normal kidney tissue ($P < 0.05$ (Fig. 1A and B). Immunohistochemistry analysis showed that CADM2 was mainly expressed in renal tubules but not glomeruli (Fig. 1C). The mRNA RT-qPCR was constant well with Western blot analyses. ($P < 0.001$) (Supplementary Fig. 1A and 1B).

### 3.2. CADM2 5′UTR is hypermethylated in both human kidney cell lines and cRCC patient specimens

To determine if the decreased expression of CADM2 is due to gene promoter methylation, *CADM2* sequences were analyzed by Methprimer program software for possible methylation sites [12]. The 5′UTR of *CADM2* contains two CpG islands (Supplementary Fig. 1C): (i) between −682 bp and −58 bp and (ii) between −1002 bp and −832 bp relative to the start codon.

Using BSP analysis, we determined the *CADM2* 5'UTR was methylated in 786-O (90.9%), OS-RC-2 (62.1%), and CAKI-1 (33.3%) cells. However, this region was generally unmethylated in HK-2 (1.5%) and HEK-293 (2.3%) cells, (Supplementary Fig. 1D), which was confirmed using MSP analysis (Fig. 2A).

Patient clinicopathological factors were next analyzed by *CADM2* promoter methylation status (Table 1; Fig. 2B and C; Supplementary Fig. 2A). Although *CADM2* promoter methylation was not correlated with patient age and sex, it was related to clinicopathological staging from pT1-pT3 ($P = 0.0012$; Table 1), suggesting that *CADM2* promoter methylation may have a role in tumor stage (pT). Notably, there was no significant difference between *CADM2* promoter methylation and Fuhrman's nuclear grade ($P = 0.157$); however, a significant difference was found between G1 and G3 ($P < 0.05$). Taken together, *CADM2* promoter methylation was associated with cRCC stage and malignancy (Supplementary Fig. 2B and C).

### 3.3. Restoration of CADM2 expression through treatment with 5-aza-dC and/or Trichostatin A (TSA)

The treatment of 5-aza-dC with or without TSA caused reactivation of *CADM2* gene expression levels in 786-O cells (Fig. 2D a and b). More interestingly, treatment with TSA alone at 100 μM can reactivate the expression of *CADM2,* but the detailed mechanism for this result has not been elucidated. The MSP results further confirm the demethylation after treatment with 5-aza-dC and/or TSA (Fig. 2D c). These data suggest that re-expression of *CADM2* occurs, at least in part, through *CADM2* demethylation and histone acetylation.

### 3.4. Determination of LOH of CADM2 in human cRCC specimens

Because LOH is an important marker for the 'two-hits' required for tumor suppressor gene inactivation [13]. We analyzed LOH in

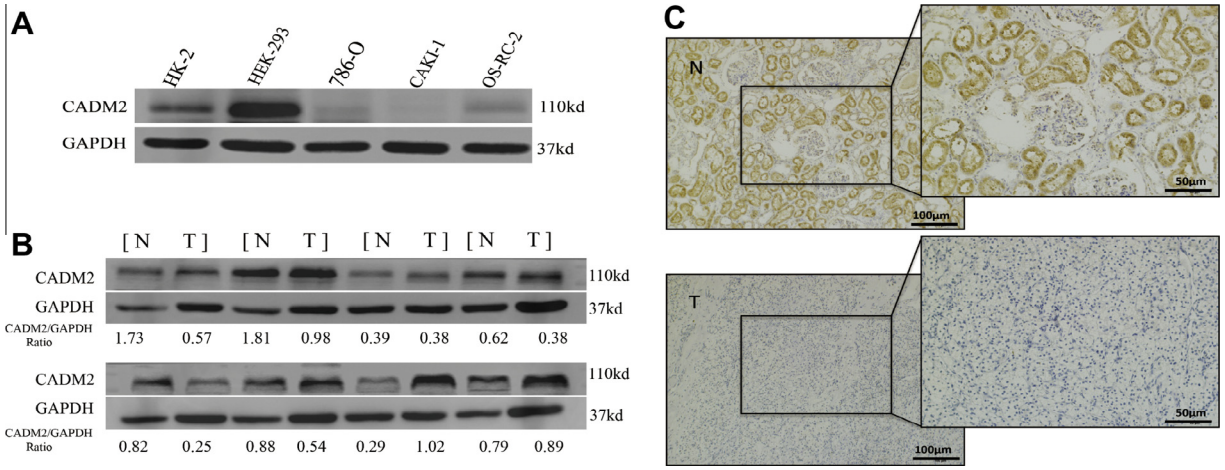


**Fig. 1.** Expression of human CADM2 in renal cell carcinoma was detected using anti-COOH-terminal antibody. GAPDH wasbed> loadedbed> as an internal control. (A) Protein expression of CADM2 decreased in cancer cell lines. (B) Endogenous CADM2 protein expression in patients specimens of cRCC wasbed> detected by Western Blot. The ratios of CADM2 band densities to relative GAPDH loading control are shown. (C) Immunohistochemical staining of cancer and normal specimens in same patients. Normal epithelium showed intense renal tubule staining, but not glomerulus; while loss of expression was showed in cancer specimens. Brown staining is indicative of CADM2 protein expression.

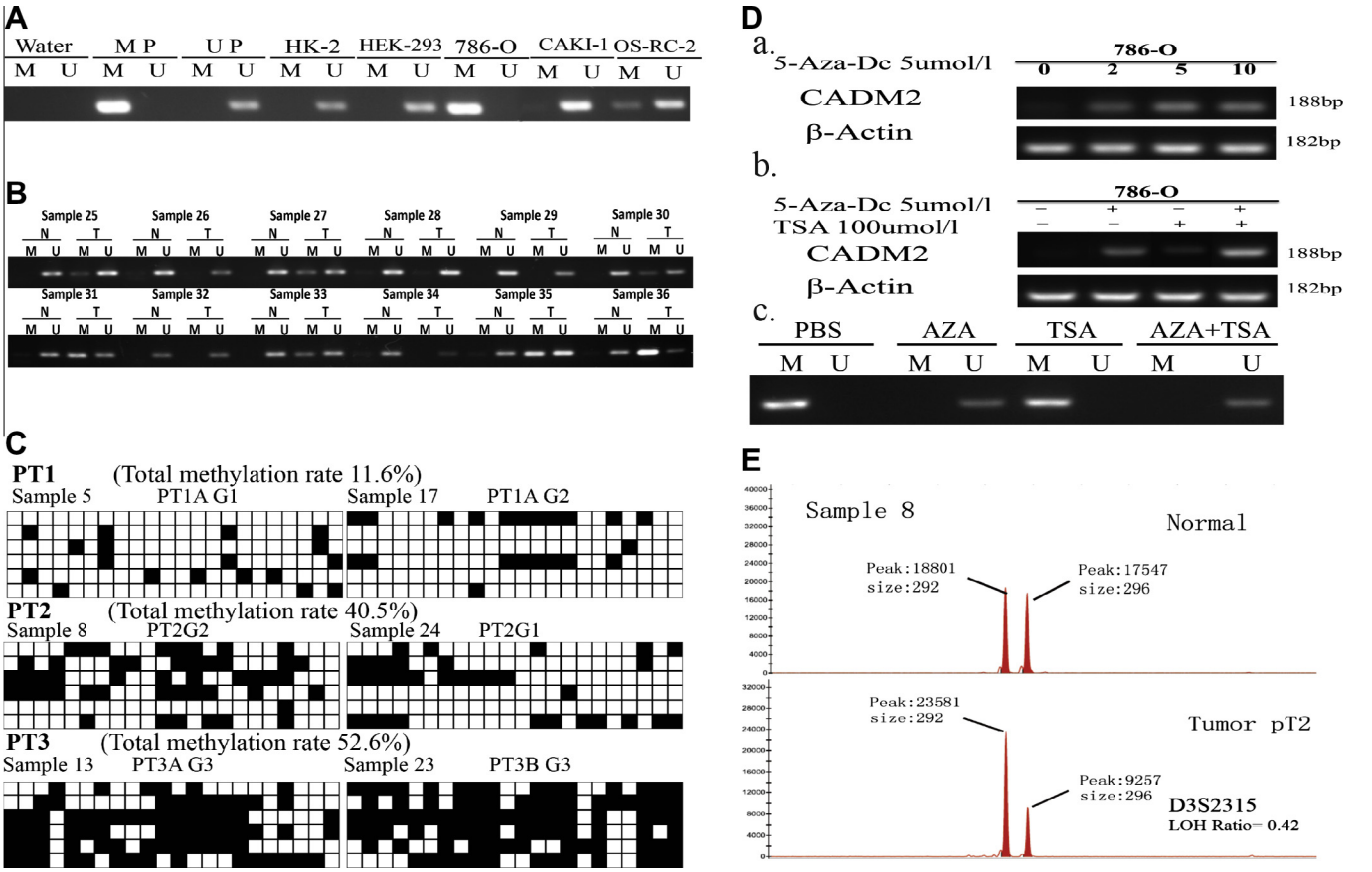


**Fig. 2.** The mechanism down-regulate the CADM2 expression in cRCC. (A) The promoter methylation in renal cell lines was determined by MSP method. MP: methylation positive control, treated with *in vitro* with M.SssI bacterial CpG methylase. UP: unmethylated positive control, DNA from normal human genomic was bisulfite converted and used as a control for unmethylated genes. Bands in lanes labeled 'U' represent unmethylated DNA while bands in lanes labeled 'M' represents methylated DNA. (B) The MSP results in cRCC specimens. (C) Bisulfite sequencing PCR (BSP) analysis for cRCC, we picked up six clones of one patient for sequencing. (D) CADM2 expression is reactivated by 5-aza-dC or TSA alone or in combination. (E) LOH assay in cRCC.

cRCC samples along with their normal controls. As shown in Fig. 2E, the ratio for tumor sample 8 was 0.42 at D3S2315. Additionally, the ratio for tumor sample number 7 is 0.34 at position SGHC-77127 (Supplementary Fig. 2D). Of the 61 patients, LOH was found in 22.4% of tumors at D3S2315, 6.7% at G32302, 3.5% at G59335 and in 5.2% and 8.6% at theSGHC-77126 and SGHC-77127, respectively (Supplementary Table 2). No significant correlations between one or more regions with LOH and pathologic parameters were observed.

### 3.5. CADM2 functions as a tumor suppressor in 786-O cells by lentivirus mediated CADM2 re-expression

To test the functions of *CADM2* in cRCC, recombinant lentiviral vectors containing *CADM2 M8* and *FL* were constructed. 786-O cells were transduced at MOI 40 for each viral vector. As shown in Supplementary Fig. 2E, protein bands were detected by western blot only in cells transduced by virus expressing *CADM2 M8* and *FL*.

To investigate the *CADM2*-mediated cell cycle effect on tumor cells the transfected 786-O cells were stained with PI. The results of FACS analyses showed increased numbers of cells in the G1 phase. The frequency of cells in G1 in the control group, mock virus group, *CADM2-M8* group and *CADM2-FL* group were 50.4 ± 1.1%, 51 ± 1.9%, 62.5 ± 1.8% and 69.3 ± 1.4%, respectively. These results suggest *CADM2* caused G1 phase arrest ($P < 0.05$) (Fig. 3A). Apoptotic cell death in 786-O cells transduced by lentiviral-*CADM2* was determined by flow cytometry. The results presented in Fig. 3B and Supplementary Fig. 2F, indicate that tumor cells transduced by lentiviral-*CADM2* underwent apoptotic cell death. The percentage of apoptotic cells in the groups was the following: control group (2.609 ± 0.39%), mock virus (4.46 ± 0.86%), lentiviral-*CADM2*-m8 (6.9 ± 0.52%), and lentiviral-*CADM2-FL* (10.92 ± 0.71%). Based on our data suggesting increased apoptosis, the activation of the caspase cascade involved in apoptosis was investigated. In most apoptotic cells, caspase-3 is an effector caspase that is activated by cleavage of the pro-caspase-3 molecule. Western blot analyses demonstrated the cleavage of PARP, a caspase-3 substrate, in cells infected with lentiviral-*CADM2* in a dose-dependent manner. These data confirm the activation of caspase enzymatic

**Table 1**
Analysis of the relationship between the clinicopathologic features and *CADM2* methylation in cRCC patients.

| | | *n* | Methylation (%) | | *P*- value |
|---|---|---|---|---|---|
| Age | <60 | 31 | 22 | 71% | |
| | ⩾60 | 30 | 18 | 60% | $P = 0.367$ |
| Gender | Male | 41 | 26 | 63.4% | |
| | Female | 20 | 14 | 70% | $P = 0.611$ |
| pT stage | pT1 | 37 | 19 | 51.4% | |
| | pT2 | 6 | 6 | 100% | |
| | pT3 | 18 | 15 | 83.3% | $P = 0.0012$ |
| Fuhrman's Nuclear grade | G1 | 16 | 10 | 62.5% | |
| | G2 | 37 | 22 | 59.5% | |
| | G3 | 8 | 8 | 100% | $P = 0.157$ |
| Total | | 61 | 40 | 65.6% | |

* Indicates a significant difference between G1 and G3 ($P < 0.05$).

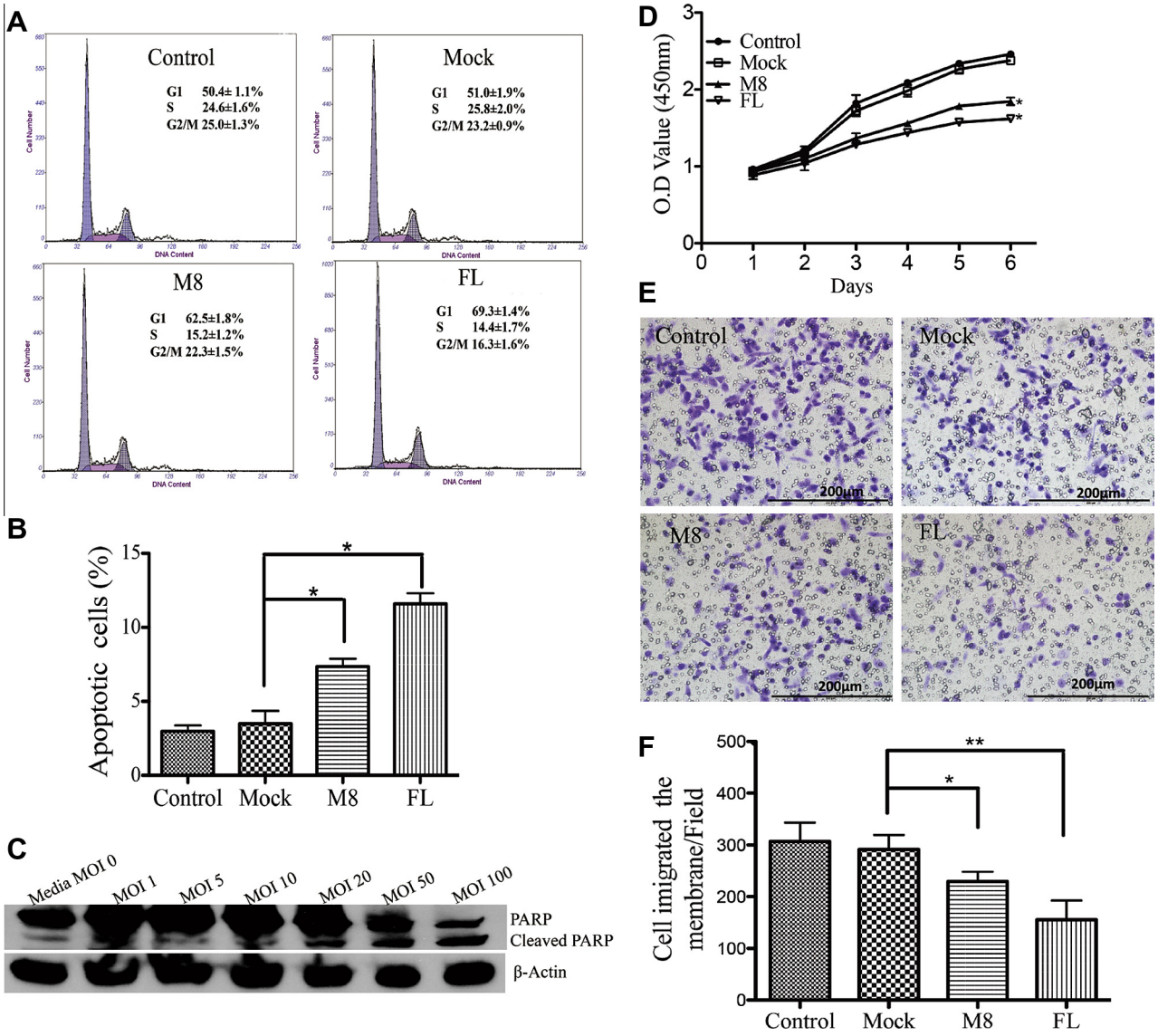


**Fig. 3.** Functional assays of CADM2 in 786-O cells after restoration of CADM2 mediated by lentiviral vector. Control: PBS. Mock: mock virus. M8: lentiviral-CADM2-M8 isoform. FL: lentiviral-CADM2-FL, at MOI 40 respectively. (A) Cell cycle analysis of infected 786-O *cells.* (B) Quantitative assessment of cell death induced by expression of *CADM2* using flow cytometry, stained with Propidium iodide (PI) or Annexin V. (C), Expression of CADM2 induces PARP cleavage through active caspase-3. (D) Effects of CADM2 on 786-O cell proliferation. 786-O cells were infected with lentiviral-CADM2 at 40 MOIs. The viability of cells was determined by CCK-8 assay. (E, F) Invasion assays. Representative images of 786-O renal cancer cells treated with virus able to cross a matrigel-coated 8 μm pore filter toward the bottom media (upper panel). Small circles are pores. A bar graph (lower panel) showing the total number of invasive cells demonstrates significant inhibition of invasion in 786-O cells following re-expression of CADM2. Error bars indicate standard error of the mean. * indicates $P < 0.05$ and ** represents $P < 0.01$ between comparison groups. The results shown are the mean of three independent experiments. (200 × magnification).

activity (Fig. 3C). A small amount of PARP cleavage was detected 3 days after infection of mock virus at an MOI of 100 due to non-specific apoptotic induction.

We used the CCK-8 assay to determine the number of viable cells at different time points after transduction with lentivirus. The results presented in Fig. 3D show that cell viability was markedly reduced for *CADM2*-transduced 786-O cells compared with control and mock-infected cells ($P < 0.05$).

The ability to migrate through a matrigel-coated filter membrane is another established *in vitro* phenotype of cancer cells. We performed invasion assays following restoration of *CADM2* in 786-O cells. *CADM2* expression decreased the number of invading cells by 27% for M8 ($P < 0.05$) and 50% for full-length ($P < 0.01$) CADM2 relative to mock virus (Fig. 3E, F). These results are consistent with our hypothesis that CADM2 suppresses renal tumor invasion after restoration in cancer cells.

### *3.6. Re-expression of CADM2 inhibits tumor growth in soft agar and in cRCC xenografts*

The introduction of tumor suppressor genes into tumorigenic cells could reverse the ability of these cells to grow in an anchorage-independent manner. To test this possibility, 786-O cells were transiently transduced and seeded in soft agar. The cells were allowed to grow for two weeks. The introduction of either the *CADM2*-m8 or *CADM2*-FL by viral vectors significantly decreased the number of colonies formed in soft agar compared with control ($P < 0.05$ for M8 and $P < 0.01$ for FL) (Fig. 4A). Consistent with this result, tumor cells expressing *CADM2* had reduced tumorigenic activity in nude mice (Fig. 4B). The tumor volumes of the mice at day 30 were significantly decreased by 64.2% in lentiviral-*CADM2-M8* and 86.3% in lentiviral-*CADM2-FL* compared to PBS or mock control ($P < 0.01$).

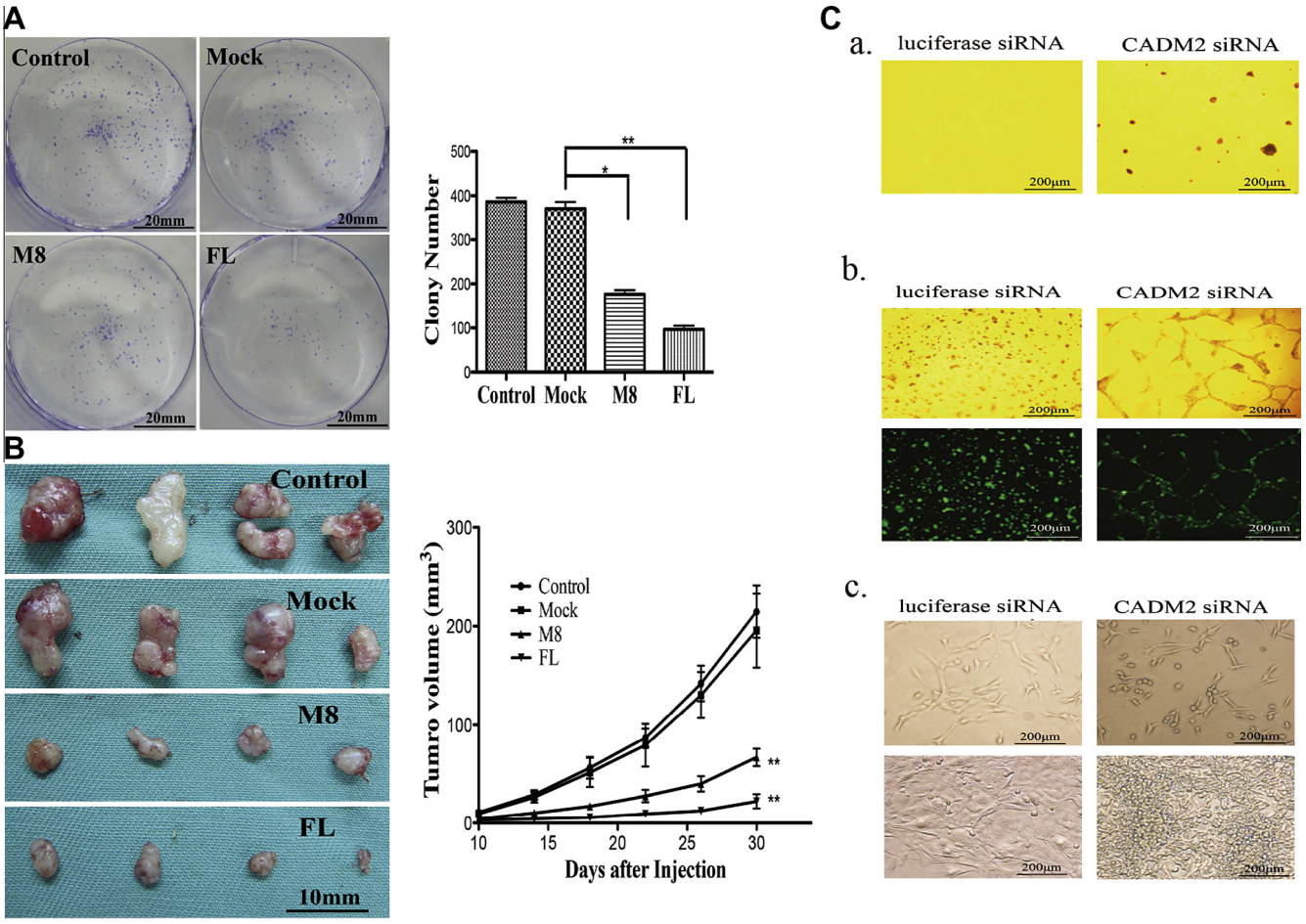


**Fig. 4.** CADM2 expression inhibits renal cancer cell tumorigenicity. (A) Representative images show that CADM2 attenuates anchorage-independent growth of 786-O cells in soft agar. Bar graph shows the mean ± SD from three independent experiments. (B) Suppression of tumor growth in nude mice by transduction of lentiviral-CADM2-M8 and CADM2-FL. Tumor growth over time for each group was shown. (C, a–c) Knockdown of CADM2 using siRNA in MDCK cells induces (a) colony formation and (b, c) morphological changes consistent with EMT. Colonies >50 μm were counted and shown in the table (200 × magnification).

### *3.7. Knockdown of endogenous CADM2 expression in MDCK cells induces tumorigenic phenotypes*

MDCK is a polarized dog kidney epithelial cell line that expresses the *CADM2* gene. The MDCK cells transfected by luciferase scramble siRNA formed only single cell colonies in soft agar (Fig. 4C). However, the colony counts (>50 μm) for *CADM2* siRNA were 238 +/− 36.1 (Fig. 4C a) ($P < 0.001$). Therefore, loss of *CADM2* induced anchorage-independent growth of MDCK cells consistent with a tumorigenic phenotype. Cells infected with *CADM2* siRNA plated on reconstituted Matrigel formed web-like aggressive structures (Fig. 4C b, right panel). Conversely, normal MDCK only form well-differentiated round spheroids (Fig. 4C b, left panel). We next assessed the morphological effects of *CADM2* siRNA on MDCK cells. The results indicated that cells stably transfected with specific *CADM2* siRNA became smaller and a more spindle shaped appearance at low density compared with scramble siRNA infected cells. These data suggest remarkable EMT changes have occurred following siRNA knockdown (Fig. 4C c, right panel). However, at higher density the cells infected with scramble siRNA grow in a monolayer, while cells with *CADM2* siRNA grow uncontrollably in a multilayer fashion and cells become more crowded and rounded. This result clearly indicates that the cells lost their contact inhibition growth arrest (Fig. 4C c, low panel). In summary, the loss of *CADM2* expression induced a tumorigenic phenotype in polarized MDCK cells.

## 4. Discussion

The cell adhesion molecule (CADM) family is a gene family whose protein expression and function have not been fully elucidated. In this study, CADM2 mRNA and protein expression was observed in cells with high polarity and adhesion, such as HK-2 and HEK-293, suggesting that CADM2 might be involved in the maintenance of cell polarity and adhesion. Similar results were also found in cRCC tissues. In normal tissues, CADM2 was mainly expressed in renal tubules but not glomeruli. This indicated that loss of CADM2 expression might be involved in the initiation and progression of cRCC, as cRCC commonly started in renal tubules.

Promoter methylation may mediate the mechanism by which CADM2 down-regulation occurs in cRCC. CADM2 promoter methylation correlated with tumor stage and grade in primary cRCC, and its expression was restored in selected cell lines after 5-aza-dC treatment. In addition, TSA induced some expression of CADM2 in 786-O cells, which is consistent with Xiong et al. [14] who reported DNA demethylation by TSA in the absence of 5-aza-dC. However, the combination of TSA and 5-aza-dC synergistically induced CADM2 mRNA expression in 786-O cells.

CADM2 expression in 786-O cells suppressed colony formation in soft agar, decreased tumorigenicity and invasion and induced apoptosis; it significantly suppressed 786-O cell growth both *in vitro* and *in vivo*. siRNA knockdown of CADM2 induced a tumorigenic phenotype in the polarized MDCK cell line in both colony

formation and 3D Matrigel growth. Cancer cells undergo EMT and lose cell polarity [15], which subsequently activates PI3-Kinase, AKT, STAT/interferon and integrin signaling pathways. Formation of an anastomosing cable-like multicellular structure by an invasive prostate cancer cell line on Matrigel can be abolished by an integrin α6 neutralizing antibody or restoration of CD82 expression, indicating a functional cross-talk between transformed cells and extracellular cell matrix (ECM) [16]. The loss of functional CADM2 is specifically responsible for the observed morphological changes observed in MDCK cells. These findings warrant further investigation to more specifically elucidate the interaction between CADM2-silenced cells and ECM, particularly interactions with Integrins and other ECM components. Mituzani et al. [17] previously reported that CADM1 interacts with integrin α(6)β(4), and inhibits disassembly of integrin α(6)β(4) from hemidesmosomes; it also plays a role in tumor suppression through hemidesmosome stabilization and inhibition of ErbB3/ErbB2 signaling. These results further support a role for CADM2 in ECM and may account for the morphological changes observed upon siRNA knockdown of CADM2 expression.

In conclusion, based on the data in this study CADM2 is a tumor suppressor that prevents the progression, invasion and metastasis of renal cancer. *CADM2* gene expression is silenced at least in part through promoter hypermethylation and/or LOH, and CADM2 promoter methylation is associated with tumor stage and grade. A more detailed mechanistic understanding of how *CADM2* plays roles in tumor suppression and its signal pathways in cRCC is required. Therefore, understanding the biologic function of *CADM2* may provide further insights into the carcinogenesis of renal cancer and lead to the identification of potential therapeutic targets.

## Acknowledgment

This project was supported by the China Health & Medical Development Foundation.

## Appendix A. Supplementary data

Supplementary data associated with this article can be found, in the online version, at http://dx.doi.org/10.1016/j.bbrc.2013.04.074.

## References

[1] L. Bastien et al., Targeted therapies in metastatic renal cancer in 2009, BJU Int. 103 (2009) 1334–1342.
[2] R. Siegel et al., Cancer statistics, 2011: the impact of eliminating socioeconomic and racial disparities on premature cancer deaths, CA Cancer J. Clin. 61 (2011) 212–236.
[3] M. Basso et al., A survey of therapy for advanced renal cell carcinoma, Urol. Oncol. 28 (2010) 121–133.
[4] M. Kuramochi et al., TSLC1 is a tumor-suppressor gene in human non-small-cell lung cancer, Nat. Genet. 27 (2001) 427–430.
[5] Y.N. Williams et al., Cell adhesion and prostate tumor-suppressor activity of TSLL2/IGSF4C, an immunoglobulin superfamily molecule homologous to TSLC1/IGSF4, Oncogene 25 (2006) 1446–1453.
[6] G. Chang et al., Hypoexpression and epigenetic regulation of candidate tumor suppressor gene CADM-2 in human prostate cancer, Clin. Cancer Res. 16 (2010) 5390–5401.
[7] N.A. Cody et al., Characterization of the 3p12.3-pcen region associated with tumor suppression in a novel ovarian cancer cell line model genetically modified by chromosome 3 fragment transfer, Mol. Carcinog. 48 (2009) 1077–1092.
[8] S.L. Lake et al., Whole-genome microarray detects deletions and loss of heterozygosity of chromosome 3 occurring exclusively in metastasizing uveal melanoma, Invest. Ophthalmol. Vis. Sci. 51 (2010) 4884–4891.
[9] D. Roy et al., Tumor suppressor genes FHIT and WWOX are deleted in primary effusion lymphoma (PEL) cell lines, Blood 118 (2011) e32–39.
[10] D.E. Hansel, Genetic alterations and histopathologic findings in familial renal cell carcinoma, Histol. Histopathol. 21 (2006) 437–444.
[11] C.A. Powell et al., Loss of heterozygosity in epithelial cells obtained by bronchial brushing: clinical utility in lung cancer, Clin. Cancer Res. 5 (1999) 2025–2034.
[12] L.C. Li, R. Dahiya, MethPrimer: designing primers for methylation PCRs, Bioinformatics 18 (2002) 1427–1431.
[13] D. Sidransky, Nucleic acid-based methods for the detection of cancer, Science 278 (1997) 1054–1059.
[14] Y. Xiong et al., Histone deacetylase inhibitors decrease DNA methyltransferase-3B messenger RNA stability and down-regulate de novo DNA methyltransferase activity in human endometrial cells, Cancer Res. 65 (2005) 2684–2689.
[15] V. Harma et al., A comprehensive panel of three-dimensional models for studies of prostate cancer growth, invasion and drug responses, PLoS ONE 5 (2010) e10431.
[16] B. He et al., Tetraspanin CD82 attenuates cellular morphogenesis through down-regulating integrin alpha6-mediated cell adhesion, J. Biol. Chem. 280 (2005) 3346–3354.
[17] K. Mizutani et al., Interaction of nectin-like molecule 2 with integrin alpha6beta4 and inhibition of disassembly of integrin alpha6beta4 from hemidesmosomes, J. Biol. Chem. 286 (2011) 36667–36676.